Effect of torsional isomerization and inclusion complex formation with cucurbit[7]uril on the fluorescence of 6-methoxy-1-methylquinolinium

Journal:	*Photochemical & Photobiological Sciences*
Manuscript ID:	PP-ART-09-2013-050307.R2
Article Type:	Paper
Date Submitted by the Author:	25-Nov-2013
Complete List of Authors:	Miskolczy, Zsombor; Institute of Molecular Pharmacology, Research Centre for Natural Sciences, Harangozó, József; Institute of Molecular Pharmacology, Research Centre for Natural Sciences, Biczók, László; Institute of Molecular Pharmacology, Research Centre for Natural Sciences, Wintgens, Véronique; Systèmes Polymères Complexes, ICMPE, Lorthioir, Cedric; Institut de Chimie et des Matériaux Paris-Est, Dpt "Systèmes Polymères Complexes" Amiel, Catherine; Systèmes Polymères Complexes, ICMPE,

Effect of torsional isomerization and inclusion complex formation with cucurbit[7]uril on the fluorescence of 6-methoxy-1-methylquinolinium

Zsombor Miskolczy[a], József G. Harangozó[a], László Biczók[a*], Véronique Wintgens[b], Cédric Lorthioir[b], Catherine Amiel[b]

[a]*Institute of Molecular Pharmacology, Research Centre for Natural Sciences, Hungarian Academy of Sciences, P.O. Box 17, 1525 Budapest, Hungary*

[b]*Systèmes Polymères Complexes, ICMPE, 2 rue Henri Dunant, 94320 Thiais, France*

Inclusion of 6-methoxy-1-methylquinolinium (C_1MQ) in the cavity of cucurbit[7]uril (CB7) was studied by absorption, fluorescence, NMR and isothermal calorimetric methods in aqueous solution at 298 K. The free C_1MQ exhibited dual-exponential fluorescence decay kinetics due to the two torsional isomers differing in the orientation of the methoxy moiety relative to the heterocyclic ring. The enthalpy-driven encapsulation of the heterocycle in CB7 led to very stable 1:1 complex with a binding constant of $(2.0\pm0.4)\times10^6$ M^{-1}. The rate of C_1MQ–CB7 complex dissociation was found to be comparable to the NMR timescale. Because the methoxy moiety is oriented outward from the host, its *s-cis–s-trans* isomerization is slightly affected by the confinement. Inclusion complex formation significantly slowed down the photoinduced electron transfer from I^- and N_3^- to the singlet-excited C_1MQ, but did not preclude the reaction because long distance electron transfer occurred through the wall of CB7 macrocycle. Due to the large difference in the quenching rate constant for free and encapsulated forms, C_1MQ is an excellent probe for the study of the inclusion of nonfluorescent compounds in CB7 in the presence of Cl^- or Br^-.

* Corresponding author. Phone: +36-1438-1103; Fax: +36-1438-1143; E-mail: biczok.laszlo@ttk.mta.hu

1. Introduction

Quinolinium derivatives are valuable fluorophores due to their high fluorescence quantum yield, applicability in wide pH range, solubility in water, and considerably Stokes-shifted emission. This moiety causes the intense fluorescence of cinchona alkaloids in strongly acidic medium.[1-5] N-Substituted 6-methoxyquinolinium cations were employed for the detection of Cl^- transport across cell membranes,[6] the fluorescence imaging of the intracellular Cl^- levels in living brain slices,[7,8] and for the characterization of the role of Ca^{2+}-dependent Cl^- channels.[9] 6-Methoxy-1-methylquinolinium was linked to a mesityl moiety to enhance Cl^- sensitivity,[10] whereas its grafting on silica nanoparticles allowed the preparation of a cell-penetrating ratiometric nanoprobe.[11] The fluorescence response to Cl^- concentration was attributed to quenching via electron transfer.[12,13] Systematic molecular structure-activity studies demonstrated that electron-donating substituent is required to achieve high chloride sensitivity.[14]

The major limitation for the quinolinium type of Cl^- sensitive fluorescent probes stands in their difficult loading into cells.[15] The encapsulation of the dye in a cell-permeable molecular container may help to overcome this problem. Therefore, we studied the thermodynamics and kinetics of confinement in a macrocycle. Cucurbit[*n*]urils are biocompatible hosts composed of *n* glycoluril units linked by a pair of methylene groups, whose inclusion complex formation can be exploited to deliver guest molecules.[16] Cellular uptake of the nanoparticles composed of substituted cucurbit[6]uril has been reported.[17] Very low toxicity was found for cucurbit[7]uril (CB7) and cucurbit[8]uril.[18,19] Their complexes were able to cross the cell membrane.[20] In the present work, the most water-soluble homologue, CB7 was used to reveal the characteristics of the inclusion complex formation with 6-methoxy-N-methylquinolinium (C_1MQ) cation, and the effect of the encapsulation on

the fluorescent behavior. Although lots of fluorescent inclusion complexes are known,[21] information regarding the effect of the host macrocycle on the electron transfer and torsional isomerization of the embedded guest is scarce. C_1MQ uniquely permits the investigation of both types of processes. On the basis of the systematic examination of C_1MQ–CB7 associate, we develop a strategy for the study of the competitive confinement of nonfluorescent compounds by probes whose fluorescence properties are insensitive to inclusion complex formation. The deeper understanding of the photoinitiated processes and inclusion in CB7 may promote the targeted delivery and efficient utilization of C_1MQ as a fluorescent probe. The formulas of the investigated substances are given in Scheme 1.

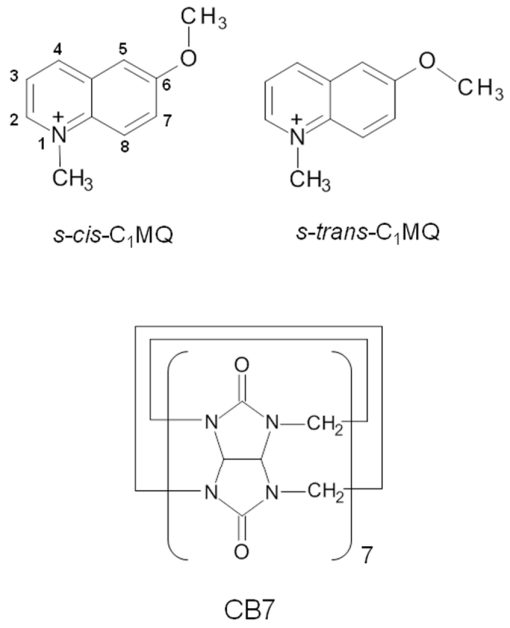

Scheme 1. Formulas of the studied compounds

2. Experimental

Iodide salt of C_1MQ was synthesized as has been reported.[22] The concentration of C_1MQ was determined spectrophotometrically on the basis of the molar absorption coefficients of 5500 $M^{-1}cm^{-1}$ at 315 nm. High purity cucurbit[7]uril[23] was kindly provided by Dr. Anthony I.

Day. The UV-visible absorption spectra were recorded on a Unicam UV 500 spectrophotometer. Fluorescence quantum yields (Φ_f) were determined relative to that of quinine sulfate in 0.5 M H_2SO_4 solution, for which a reference yield of $\Phi_f = 0.546$ was taken.[24] Corrected fluorescence spectra were obtained on a Jobin-Yvon Fluoromax-P spectrofluorometer. Fluorescence decays were measured with a time-correlated single-photon counting technique on a previously described apparatus.[25] Data were analyzed by a non-linear least-squares deconvolution method with Picoquant FluoFit software. Quantum chemical calculations were performed with RM1 method using HyperChem 8.0 program (Hypercube Inc., Gainesville, FL). Isothermal titration calorimetry (ITC) measurements were carried out with a MicroCal VP-ITC microcalorimeter at 298 K as have been reported elsewhere.[26] NMR spectra were taken on a Bruker Avance II 400 MHz NMR spectrometer, equipped with a 5 mm ^{1}H/X probe. The error limits represent standard deviation.

3. Results and Discussion

Photophysical properties in water

The absorption and fluorescence spectra of C_1MQ resemble that of quinine sulfate in strongly acidic medium. (Supporting Information, Figure S1) The absorption maxima around 316 and 345 nm in water are attributed to transitions to S_2 and S_1 singlet excited states on the basis of the analogous spectrum of quinine sulfate in 0.5 M H_2SO_4 aqueous solution.[27,28] Excitation at the red edge of the C_1MQ absorption band (415 nm) led to about 10 nm bathochromic displacement of the fluorescence peak. The excitation spectrum moved to a smaller extent to lower energy when the detection wavelength was changed from 400 to 500 nm (Supporting Information, Figure S2). These phenomena indicate the existence of two species in the ground and excited states, which correspond to *s-cis*-C_1MQ and *s-trans*-C_1MQ (Scheme 1).[29]

Two distinct isomers have also been reported for 2-methoxynaphthalene[30] and 2-methoxyanthracene.[31]

RM1 semiempirical calculations using HyperChem 8.0 program showed that the energy of the *s-cis* form is about 4 kJ mol^{-1} lower in the ground state. This is in accord with the *s-trans–s-cis* energy difference of 4.82 kJ mol^{-1} found by NMR for 2-methoxynaphthalene.[32] The calculated electron density distribution of the heterocyclic ring significantly differs for the two C_1MQ isomers. The partial charge at the position 5 is more negative for the *s-cis* form, whereas higher electron density is obtained at the position 7 in the case of *s-trans*-C_1MQ. The calculations also showed that the dipole moment component along the long axis of the aromatic ring is larger for *s-cis*-C_1MQ.

Time-resolved fluorescence measurements exhibited dual-exponential decay kinetics. Deaeration of the solution insignificantly affected the fluorescence lifetimes implying very slow quenching of the singlet-excited molecules by oxygen. The fluorescence signals were concentration-invariant indicating that C_1MQ aggregation did not take place. The time-dependence of the fluorescence intensity could be well described with a sum of two exponential functions ($I(t)=A_1\exp(-t/\tau_1)+A_2\exp(-t/\tau_2)$). The fluorescence lifetimes (τ_1 and τ_2) listed in Table 1 did not change with the detection wavelength within the limits of experimental errors (ca. ±4%), but the relative contribution of the amplitude of the longer-

Table 1. Fluorescence characteristics of C_1MQ in water and CB7 cavity

	Φ_F	τ_1 / ns	τ_2 / ns	$A_1/(A_1+A_2)$ at 500 nm
C_1MQ	0.46	19.4	37.1	0.72
C_1MQ–CB7	0.50	28.3	46.3	0.81

lived component gradually increased towards longer wavelengths. Both amplitudes were positive irrespective of the detection wavelength. The lack of initial build-up indicates that the equilibrium between the two torsional isomers does not alter significantly upon excitation and/or the interconversion between the *s-cis* and *s-trans* excited forms is much faster than the lifetime of their excited states. Figure 1 displays the time-resolved area-normalized emission spectra (TRANES)[33] constructed from the fluorescence decays of C_1MQ at various wavelengths. The fluorescence maxima are located at 441 and 450 nm at 0 and 100 ns after the excitation, respectively. The appearance of an isoemissive point at 447 nm proves that the nonexponential decay kinetics is not due to solvation dynamics. This is in sharp contrast to the continuous red-shift of the spectra with increasing time reported for 6-methoxyquinolinium[34] and double protonated quinidine[35] in 1 N H_2SO_4 glycerol-water 1:1 mixture as well as for 6-methoxyquinoline at pH 12 in water[36]

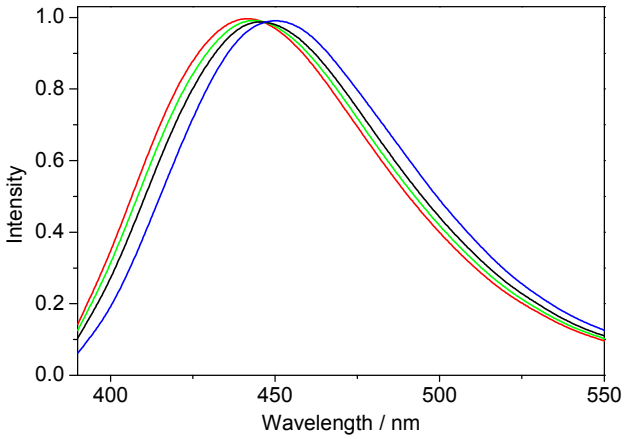

Figure 1. Time-resolved area-normalized fluorescence spectra of C_1MQ in water at 0 (red), 25 (green), 50 (black), and 100 ns (blue) after excitation at 372 nm.

and quinine sulfate in 1 N H_2SO_4 aqueous solution.[37] The lower-energy emission of the TRANES spectra, which has longer lifetime, is assigned to singlet-excited *s-trans*-C_1MQ because the excitation at the red edge of the absorption spectrum, where ground state *s-trans*-

C_1MQ preferentially absorbs, induces this fluorescence. The shorter-lived *s-cis*-C_1MQ emission dominates at the blue edge of the fluorescence band. The energy gap between S_1 and S_0 states ($E_{0\text{-}0}$) was estimated from the intersection of the normalized excitation and TRANES spectra (Supporting Information, Figure S2). The $E_{0\text{-}0}$ values were found to be 25650 and 26060 cm^{-1} (3.18 and 3.23 eV) for *s-trans*- and *s-cis*-C_1MQ, respectively.

Inclusion of C_1MQ in CB7 cavity

Figure 2 presents the results of spectrophotometric titration of 31 μM C_1MQ with CB7 in water. The addition of CB7 leads to marked alteration in the absorption spectrum, and isosbestic points develop at 256, 273, and 357 nm. The bathochromic shift and the hypochromicity of the bands are evidence of host-guest complex formation. The absorbance

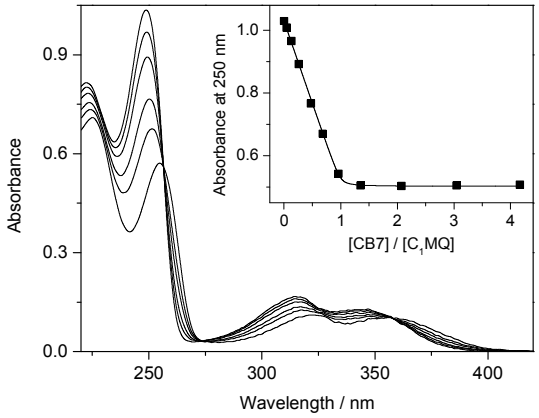

Figure 2. Alteration of the absorption spectrum of 31 μM C_1MQ upon addition of 0, 4.1, 8.1, 15, 21, and 42 μM CB7 in water. Inset: absorbance at 250 nm as a function of [CB7]/[C_1MQ] molar ratio.

at 250 nm exhibits an initial linear decrease followed by a CB7 concentration independent domain (inset to Figure 2). A sharp break appears at equimolar concentration of C_1MQ and CB7 indicating 1:1 binding stoichiometry. The equilibrium constant of complexation cannot

be determined accurately when the concentration dependence of the measured quantity consists of two portions of straight lines.[38] Therefore, fluorescence spectroscopic measurements were performed, which allowed much more diluted solutions to be studied. Figure 3 displays the change of the fluorescence spectra with the increase of CB7 concentration in 0.37 μM C_1MQ solution. The samples were excited at the isosbestic point at

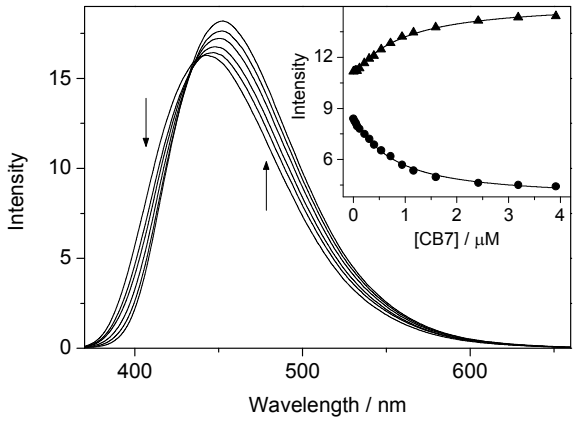

Figure 3. Fluorescence spectrum of 0.37 μM C_1MQ in the presence of 0, 0.31, 0.54, 0.94, 1.6, and 3.2 μM CB7 in aqueous solution. Excitation at 357 nm, slits 5 nm. Inset: fluorescence intensity vs. CB7 concentration at 407 (●) and 480 nm (▲). The line represents the result of the global analysis in the 370-650 nm range.

357 nm. The intensity of the band slightly grew and the location of the maximum shifted from 444 to 452 nm. The fluorescence quantum yields (Φ_F) were found to be 0.46 and 0.50 for the free and complexed C_1MQ, respectively. The fluorescence decay kinetics remained dual exponential in CB7 cavity indicating that the methoxy substituent can have *s-cis* and *s-trans* conformation even after complexation. The fluorescence lifetimes of C_1MQ–CB7 complex became longer compared to those of free C_1MQ. (Table 1.) The very low polarizability inside the CB7 cavity[39] slightly diminishes the rate constants of fluorescence and radiationless deactivation for *s-cis*- and *s-trans*-C_1MQ alike. Interestingly, the

encapsulation in CB7 decreases the amplitude of the fluorescence of the *s-trans* form. This implies that the *s-trans–s-cis* energy gap grows upon inclusion complex formation probably both in the ground and singlet-excited states. The TRANES spectra resembles those of uncomplexed C_1MQ (Supporting Information, Figure S3), but the maximum shifts to a smaller extent from 451 nm to 455 nm at 0 and 100 ns after excitation, respectively. The isoemissive point is observed at 462 nm.

Equilibrium constant of inclusion complex formation (K) was calculated by the nonlinear least-squares fit of fluorescence intensities (I) by the following function:

$$I = I_0 + \frac{I_\infty - I_0}{2}\left\{1 + \frac{[CB7]_0}{[C_1MQ]_0} + \frac{1}{K[C_1MQ]_0} - \left[\left(1 + \frac{[CB7]_0}{[C_1MQ]_0} + \frac{1}{K[C_1MQ]_0}\right)^2 - 4\frac{[CB7]_0}{[C_1MQ]_0}\right]^{\frac{1}{2}}\right\} \quad (1)$$

where I_∞ and I_0 denote the intensity for the fully complexed and free C_1MQ, $[CB7]_0$ and $[C_1MQ]_0$ represent the total concentration of the host and guest compounds, respectively. The global analysis of the experimental data in the 370–650 nm range provides $K = (1.8\pm0.2)\times10^6\ M^{-1}$. The inset in Figure 3 shows the quality of the fit at two representative wavelengths. The strong binding stems from the combined effects of ion-dipole and hydrophobic host-guest interactions within the nonpolar cavity of CB7.

Effect of CB7 on the fluorescence quenching by anions

To reveal how electrolytes influence the fluorescence decay kinetics of singlet-excited C_1MQ (C_1MQ^*) time-resolved fluorescence was detected at 550 nm, where both *s-cis*- and *s-trans*-C_1MQ* emit. Among the various sodium salts, $NaClO_4$ caused negligible effect in the 0 – 0.3 M concentration range, whereas addition of sodium halides to C_1MQ aqueous solution markedly accelerated the fluorescence decay. The reciprocal lifetime of both torsional

isomers ($1/\tau$) showed linear correlation with anion concentration and the slope corresponds to the rate constant of quenching (k_q):

$$1/\tau = 1/\tau_0 + k_q[\text{anion}] \quad (2)$$

where τ_0 denotes the lifetime in neat water. Table 2 summarizes k_q values and reports the oxidation potential of the various anions (E_{ox}). Jayaraman and Verkman demonstrated that anions quench the fluorescence of substituted N-methylquinolinium cations via electron transfer, but the effect on the fluorescence decay was not examined.[12] We always found larger k_q for *s-cis*-C_1MQ^* quenching both for the encapsulated and free species. This trend is probably due mainly to the larger energy gap between S_1 and S_0 states in the case of *s-cis*-C_1MQ^* (vide supra).

Table 2 Quenching rate constants of *s-cis*- and *s-trans*-C_1MQ* by different anions with their oxidation potentials

Anion	E_{ox} V vs. NHE[a]	*s-cis*-C_1MQ^*			*s-trans*-C_1MQ^*		
		ΔG / eV	k_q / 10^8 $M^{-1}s^{-1}$		ΔG / eV	k_q / 10^8 $M^{-1}s^{-1}$	
		in H_2O	in H_2O	in CB7 solution[b]	in H_2O	in H_2O	in CB7 solution[b]
I^-	1.33	-0.98	260	5.4	-0.93	230	2.6
N_3^-	1.35	-0.96	260	1.6	-0.91	210	0.57
Br^-	1.92	-0.39	220	[c]	-0.34	190	[c]
Cl^-	2.50	0.19	91	[c]	0.24	27	[c]

[a]Reference[40], [b][C_1MQ] = 0.023 mM and [CB7] = 0.25 mM, [c]negligible quenching

The free enthalpy change in the photoinduced electron transfer reaction (ΔG) can be estimated as[41]

$$\Delta G = E_{ox} - E_{red} - E_{0-0} + C \quad (3)$$

E_{0-0} denotes the energy of the singlet-excited state. E_{red} = -0.84 V vs. NHE is derived from the reported[12] reduction potential of C_1MQ using 0.22 V for the standard potential of the Ag/AgCl electrode.[42] The same E_{red} is assumed for *s-cis*- and *s-trans*-C_1MQ. The Coulomb term (C), which accounts for the effect of the electrostatic attraction of the reactants is negligible in water. The calculated ΔG values are summarized in Table 2. Because of the substantial driving force of electron transfer, the reactions with I^-, N_3^- and Br^- are close to diffusion controlled. A small increase of k_q with decreasing ΔG has been found for highly exergonic electron transfer in qualitative agreement with theories.[43] The much slower quenching with Cl^- arises from the positive ΔG of the reaction.

Surprisingly, complexation with CB7 does not preclude the reaction with I^- and N_3^- despite the almost complete embedment of the heterocyclic ring of C_1MQ in the hydrophobic core of the host (vide infra). After the encapsulation of C_1MQ no space remains for the coinclusion of anions. CB7 prevents the contact between embedded C_1MQ and anions. However, through-space electron transfer can occur at long range when the driving force is large. Because of the deceleration of the electron transfer with the donor-acceptor separation distance, k_q values for C_1MQ^*–CB7 complexes are much smaller than those of free C_1MQ^*. The electrostatic repulsion between the anions and the large electron density of the carbonyl oxygen atoms at the portals of the macrocycle hinders the access of C_1MQ^* by anions from the direction of the opening of CB7. However, the partially positive charge of carbons located at the symmetry plane of CB7 promotes the approach by anions facilitating thereby the long distance electron transfer from I^- and N_3^- to the CB7-embedded C_1MQ^*. The effective separation interval, at which the electron transfer can takes place, becomes smaller when ΔG is increased. Br^- and Cl^- cannot reach this distance due to the protection of C_1MQ^*

by the host macrocycle. Consequently, they are not able to react with the encapsulated C_1MQ^*. Nau and coworkers have also observed significant deceleration of fluorescence quenching upon embedment in CB7.[44] The rate constant of singlet-excited 2,3-diazabicyclo[2.2.2]oct-2-ene–CB7 complex interaction with I^- was found to be[44] less then 5×10^6 $M^{-1}s^{-1}$. The much more rapid reaction of C_1MQ^*–CB7 associate with I^- originates probably from the more negative ΔG of electron transfer to the positively charged excited guest.

Utilization of C_1MQ as a fluorescent probe

The small difference between the fluorescent properties of free and CB7-confined C_1MQ in neat water (Figure 3) substantially increases in the presence of Br^- or Cl^- because these anions selectively quench the unbound C_1MQ, but do not react with C_1MQ^*–CB7 inclusion complex. Therefore, the competitive binding of a nonfluorescent compound in CB7 can be sensitively detected by the change of the C_1MQ fluorescence intensity in the solution of Br^- or Cl^-. When a competitor expels C_1MQ from the cavity of CB7, the intense fluorescence is quenched by these anions and the binding constant of the competitor can be determined from the fluorescence intensity diminution.

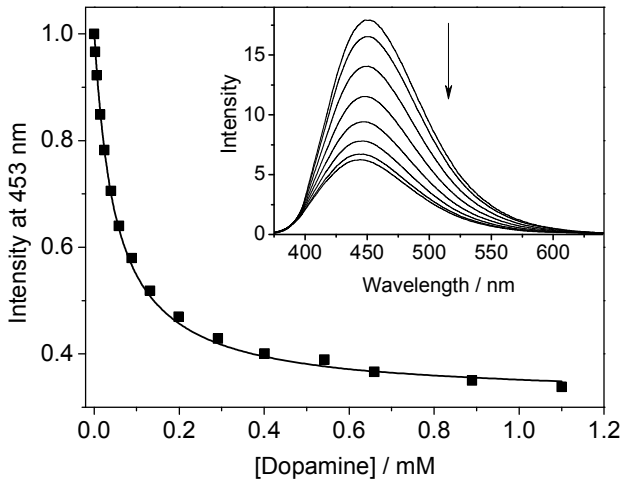

Figure 4. Change of the intensity at 453 nm and the spectra of fluorescence (inset) with increasing $DOPAH^+$ concentration in 25 mM NaCl aqueous solution. [C_1MQ] = 1.1 μM, [CB7] = 3.4 μM and [$DOPAH^+$] in the inset 0, 6.0, 24, 58, 130, 290, 660, 1100 mM. Excitation was at 357 nm. The line through the experimental points represents the fitted function (see text and ref.45 for the adopted fitting procedure).

As a proof of concept, the results with dopamine hydrochloride are displayed in Figure 4. The blue-shift of the fluorescence band indicates that C_1MQ is gradually released from CB7 cavity when protonated dopamine ($DOPAH^+$) concentration is raised, and the fraction of the encapsulated $DOPAH^+$ grows. The substantial intensity diminution originates from the efficient quenching of the uncomplexed C_1MQ^* via electron transfer with Cl^-. $DOPAH^+$ does not absorb at the excitation wavelength (357 nm), and its low concentration does not permit reaction with C_1MQ^*. The experimental data were analyzed with a home-made MATLAB program as described in our previous paper.[45] $K = (3.8\pm0.2)\times10^5\ M^{-1}$ was used for the equilibrium constant of C_1MQ inclusion in CB7 in the presence of 25 mM NaCl. This K value was obtained from a fluorescence titration in the absence of dopamine. The slightly lower binding constant in NaCl solution compared to that in water results from the coordination of Na^+ to the carbonyl-fringed portals of CB7, which hinders the confinement of C_1MQ.[46-48] The nonlinear least-squares fit of the data in Figure 4 provided $(5.2\pm0.7)\times10^4\ M^{-1}$ for the binding constant of $DOPAH^+$ in CB7 in the presence of 25 mM NaCl.

Thermodynamics of inclusion in CB7

Isothermal calorimetric titrations provided information on the thermodynamics of encapsulation of C_1MQ in CB7. A representative result is presented in Figure 5. Upon

successive addition of 0.7 mM C_1MQ solution into 0.08 mM CB7 in water, the quantity of released heat per mole of injectant is proportional to the extent of binding. As CB7 becomes saturated with C_1MQ, the signal vanishes. The inflexion point appears around 1:1 molar ratio confirming the equimolar complexation stoichiometry. The nonlinear least-squares analysis of the experimental data with the one site model provided $\Delta H = -37.0$ kJ mol^{-1} for the enthalpy of complexation. Because of the steep change of the binding isotherm with

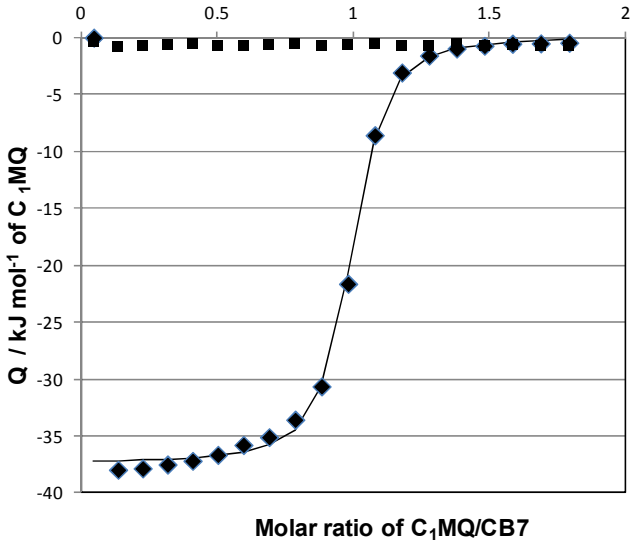

Figure 5. ITC profile of injections of 0.7 mM C_1MQ into 0.08 mM CB7 solution (◆) and into water (■). The line represents the results of the fit with a one site model.

[C_1MQ]/[CB7] ratio around the inflexion point, only a lower limit ($K > 10^6$ M^{-1}) was obtained for the binding constant. It is known that the product of K and the ligand concentration should stand in the range 10-500 for ITC experiments.[49,50] To determine accurate K value, displacement assay[51] was carried out using the competitive inclusion of 1,3-dimethylimidazolium cation (C_1mim$^+$) in CB7 as a reference because it has a well-established equilibrium constant[26,52] ($K = 7.5\times10^4$ M^{-1}). The titration of 0.08 mM CB7 and 0.13–0.20 mM C_1mim$^+$ solutions with 0.7 mM C_1MQ gave $K = (2.2\pm0.2)\times10^6$ M^{-1} for the

stability constant of C_1MQ–CB7 complex in fair agreement with the corresponding quantity ($K=(1.8\pm0.2)\times10^6$ M^{-1}) derived by fluorescence method (vide supra). Knowing ΔH and K enables the calculation of the standard free enthalpy (ΔG) and entropy (ΔS) changes upon confinement in CB7 according to the equation

$$\Delta G = -RT \ln K = \Delta H - T\Delta S \quad (2)$$

where R is the gas constant and T is the temperature. ΔG = -35.9 kJ mol^{-1} was obtained for the standard free enthalpy. The substantial enthalpy gain, ΔH= -37.0 kJ mol^{-1} indicates that confinement of C_1MQ in CB7 is an enthalpy-controlled process. The entropic contribution to the driving force is slightly negative ($T\Delta S$ = -1.1 kJ mol^{-1} at 298 K). It has been demonstrated that the release of high-energy water from the cavity of cucurbit[n]uril macrocycles plays a decisive role in the stabilization of the inclusion complexes of neutral guests.[53] In the case of the cationic C_1MQ, electrostatic interactions with CB7 also contribute to the significant enthalpy diminution upon encapsulation.

Structure of C_1MQ–CB7 complex

RM1 semiempirical calculations with HyperChem 8.0 program provided information on the position of C_1MQ in CB7 macrocycle. In the energy-minimized structure (Figure 6), the aromatic quinolinium and the methyl substituent of the heterocyclic nitrogen are located in the apolar core of CB7, whereas the methoxy group protrudes into the aqueous phase.

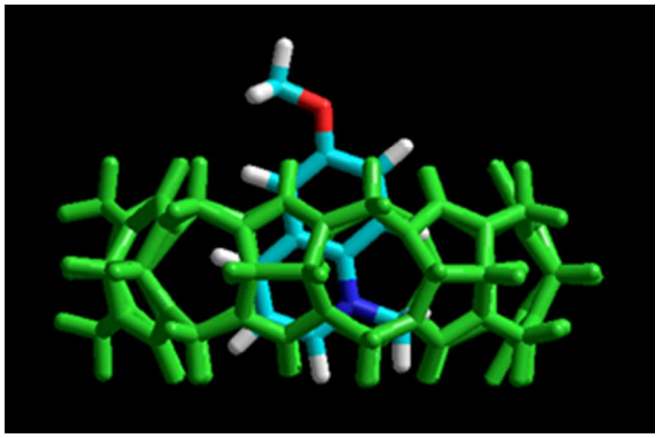

Figure 6. Structure of *s-cis*-C_1MQ–CB7 inclusion complex in the ground state calculated by RM1 semiempirical method. Color codes: CB7, green; C_1MQ, oxygen, red; nitrogen, blue; carbon, light blue and hydrogen, white.

Among the aromatic hydrogen atoms, those in the positions 4 and 8 are the ones the most deeply embedded within the macrocycle. The calculations show that the charge of C_1MQ is delocalized. The carbon atom at the position 6 has the most substantial positive partial charge, which interacts with the high electron density of the oxygen atoms at the portal of CB7. Considerable electron density in the aromatic ring of C_1MQ is found in the positions 5 and 3, which are in the vicinity of the planes of the electron deficient carbon atoms of the CO groups of CB7. The interaction of the partial positive charge of the aromatic hydrogen atoms with the considerable negative electrostatic potential of the inner surface of the macrocycle[54] also contributes to the stability of the C_1MQ–CB7 complex. Because the methoxy substituent is located outside the host, the inclusion complex formation only slightly influences the *s-trans*–*s-cis* torsional isomerization.

NMR spectra and complexation kinetics

The calculated structure was confirmed by ^{1}H NMR measurements. Figure 7 depicts the ^{1}H NMR spectra of C_1MQ in D_2O in the absence and presence of 1.35 equivalents of CB7. The assignment of the resonances in Figure 7A, originating from ^{1}H–^{1}H COSY and NOESY experiments (Supporting Information, Figure S4, S5), is in qualitative agreement with reported chemical shift values.[10] Because of the rapid isomerization, the O–CH_3 signals for *s-cis*- and *s-trans*-C_1MQ are indistinguishable on the ^{1}H NMR spectrum. Upon addition of more than one equivalent of CB7 to C_1MQ solution, the resonances related to all aromatic and N–CH_3 protons are significantly shifted upfield (Figure 7B) indicating the encapsulation in CB7. In contrast, the peak attributed to the O–CH_3 protons slightly moves downfield suggesting that this moiety is located near to the carbonyl portal outside the CB7 cavity. Table 3 summarizes the CB7-induced chemical shift variation (Δδ) of the C1MQ protons.

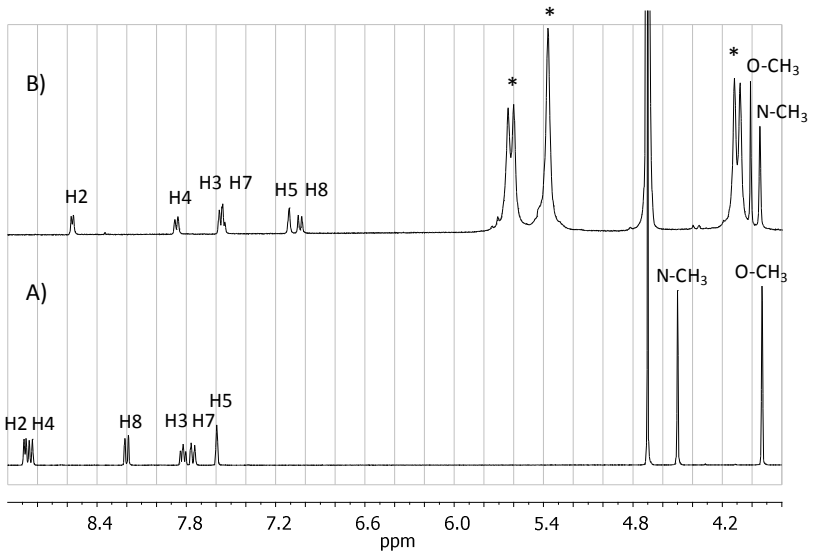

Figure 7. ^{1}H NMR spectra of (A) 0.7 mM C1MQ and (B) after addition of 1.35 equivalent CB7 in D_2O. (* denotes the peaks related to the CB7 protons)

Table 3. Displacement of proton resonances upon the confinement of C_1MQ in CB7

	H2	H3	H4	H5	H7	H8	N–CH_3	O–CH_3
Δδ (ppm)	-0.321	-0.298 -0.233	-0.981	-0.484	-0.230 -0.165	-1.168	-0.557	0.074

The largest changes appear for the signal of the protons located at the positions 4 and 8 of the quinolinium ring. This implies, in accordance with the calculated structure of C_1MQ–CB7 complex (Figure 6), that these two hydrogen atoms occupy, on average, the innermost position in CB7.

Figure 8 displays the variation of the aromatic resonances observed on the ^{1}H NMR spectrum upon gradual increase of CB7:C_1MQ molar ratio. Because of the large equilibrium constant of C_1MQ–CB7 complex formation (K=(2.0±0.4)×10^6 M^{-1} vide supra), nearly all

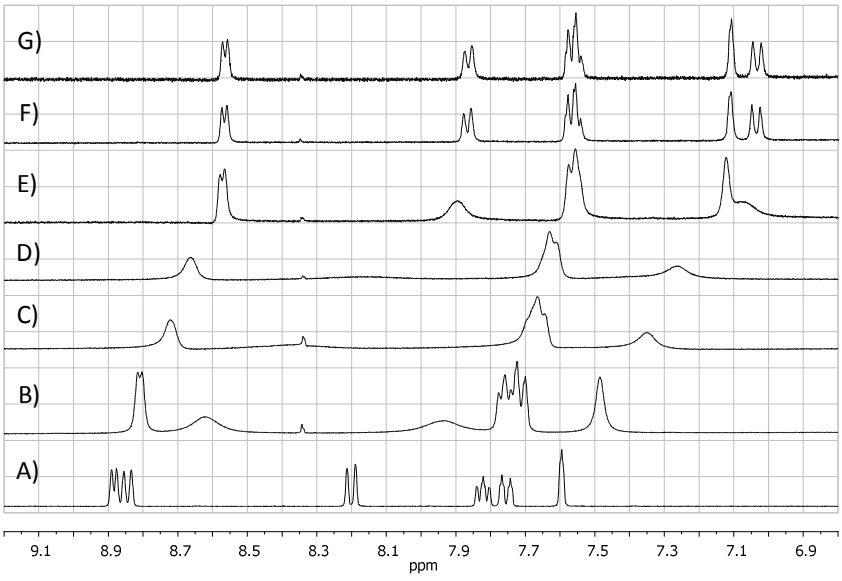

Figure 8. Aromatic proton resonance region of ^{1}H NMR spectra at [CB7]:[C_1MQ] molar ratio of 0 (A), 0.22 (B), 0.47 (C), 0.62 (D), 0.88 (E), 1.35 (F) and 3.12 (G) in D_2O.

C_1MQ molecules are encapsulated in CB7 at the equimolar solution of the components. Therefore, the spectra in Figure 8F and G barely differ, and are assigned to C_1MQ–CB7 inclusion complex. When the CB7:C_1MQ molar ratio is decreased from 1 to 0, a continuous displacement of the aromatic proton resonances is observed (Figure 8A-E). The line width also undergoes significant changes, reaching the largest broadening around CB7:C_1MQ molar ratio of 0.6. The resonances assigned to H4 and H8 become so broad that they can hardly be detected. Such a behavior of both chemical shift and line width implies that the rate of the exchange between bound and free C_1MQ is comparable to the NMR time scale, which can be expressed in this kind of experiments as $\tau_c = \left[2\pi\nu_0\left|\delta_b - \delta_f\right|\right]^{-1}$, i.e. about 1 ms.[55] In this equation, ν_0 stands for the ^{1}H Larmor frequency, whereas δ_b and δ_f denote the ^{1}H chemical shift for bound and free C_1MQ, respectively. Yu and coworkers investigated[56] a series of cyclohexane derivatives in presence of CB7, and found that the relative contributions of hydrophobic interactions and ion-dipole/hydrogen bonding interactions influence both the thermodynamic constant and the exchange rate between the host and the guest. In the case of C_1MQ hydrogen bonding is not possible with the host. The structure of the complex (Figure 6) permits a good balance between the hydrophobic interaction within the CB7 cavity and the interactions of the partial charges in the portal region and inside CB7.

The kinetic parameter τ of the exchange has the following relationship with the mean lifetime of the bound (τ_b) and free (τ_f) C_1MQ:

$$1/\tau = 1/\tau_b + 1/\tau_f \qquad (3)$$

In the case of intermediate exchange, close to the coalescence point, τ can be derived from the effect of the exchange on the ^{1}H NMR line width $\delta\nu$ by the following equation:[55]

$$\delta\nu - \delta\nu_0 = 4\pi p_f p_b \tau/\tau_c^2 \qquad (4)$$

where $\delta\nu_0$ stands for the line width in the absence of exchange phenomena, which is estimated from the ^{1}H NMR spectra of C_1MQ in D_2O (Figure 8A), whereas p_f and p_b denote the molar fraction of free and bound C_1MQ molecules. On the basis of equation 4, τ = 0.25 ms was obtained from the line width of the H4 resonance at the CB7:C_1MQ molar ratio of 0.62 (Figure 8C) at 297 K. From this τ value, $k_d = 1.5\times10^3$ s^{-1} is calculated for the rate constant of the dissociation of C_1MQ–CB7 complex using the relationship[55] $k_d = 1/[(1+p_b/p_f)\tau]$. The rate constant of the inclusion complex formation $k_a = 3.0\times10^9$ $M^{-1}s^{-1}$ is derived from the average of the binding constant determined by fluorescence and ITC measurements $K=k_a/k_d = (2.0\pm0.4)\times10^6$ M^{-1}. Surprisingly, the rate constant of association is not far from the diffusion-controlled limit of bimolecular reactions (6.5×10^9 $M^{-1}s^{-1}$) in water.[57] This suggests that the relatively small C_1MQ can easily enter into CB7 without significant steric hindrance and structural alteration of the reactants. No significant barrier has to be overcome before inclusion. Moreover, the release of water from CB7 cavity and from the hydrate shell of C_1MQ seems to require insubstantial activation energy. The k_a found in this study closely agrees with the corresponding values published for the ingress of singlet-excited 2-naphthol[58] (2.5×10^9 $M^{-1}s^{-1}$), triplet-excited chromone[59] (3×10^9 $M^{-1}s^{-1}$) and triplet-excited flavone[59] (2.4×10^9 $M^{-1}s^{-1}$) into β-cyclodextrin (β-CD). Because of the weaker host-guest interactions, the latter two β-CD complexes dissociate much more rapidly than C_1MQ–CB7, which has a considerable negative binding enthalpy (vide supra). The larger apolar ring system of singlet-excited 2-naphthol give rise to stronger association with β-CD. Therefore, the exit rate constant from this complex[58] (522 s^{-1}) is similar to that obtained for C_1MQ–CB7. Bohne and coworkers showed that formation of a complex between a positively charged guest and CB7 can occur at a rate close to the diffusion-controlled limit without

detectable intermediate.[60] The association rate constant of 6.3×10^8 $M^{-1}s^{-1}$ was found for the confinement of R-(+)-2-naphthyl-1-ethylammonium in CB7.[60]

4. Conclusions

The dual fluorescence of C_1MQ is due to two torsional isomers, which differ in the orientation of the methoxy substituent. Such a sometimes overlooked phenomenon may also contribute to the intricate photophysics of methoxyquinoline type of alkaloids. The relative amounts of the two fluorescence components are barely affected by inclusion in CB7 cavity because the methoxy moiety of C_1MQ is located outside the macrocycle in the aqueous phase. When methoxyquinolinium fluorophores are employed as probes in various environments, it has to be taken into account that the rate constant of fluorescence quenching can markedly differ for the *s-cis* and *s-trans* forms. Therefore, the results may alter with the detection wavelength, which influences the accuracy of quantitative analysis. The remarkably stable 1:1 binding of C_1MQ with CB7 is an enthalpy-driven process, and the slow dissociation of the produced inclusion complex is responsible for the high binding constant. The cooperativity of the hydrophobic effects and dipole interactions decelerates the C_1MQ exchange in CB7. The close to diffusion-controlled rate constant of the confinement in CB7 is advantageous in the utilization of C_1MQ as a fluorescence probe for the examination of the competitive encapsulation of nonemitting compounds. The enormous difference in reaction rate of the free and CB7-embedded singlet-excited C_1MQ in the electron transfer from Cl^- or Br^- can be exploited to sensitively detect the release of C_1MQ from CB7.

Acknowledgment

We appreciate the support of this work by the Hungarian Scientific Research Fund (OTKA, Grant K104201) and the bilateral program between CNRS and the Hungarian Academy of Sciences.

References

1 N. Kumar Joshi, R. Rautela, H. C. Joshi and S. Pant, Fluorescence studies of some protonated cinchona alkaloids in polymers, *J. Luminesc.*, 2011, **131**, 1550-1555.

2 S. Pant, D. Pant and H. B. Tripathi, Photophysics of the dications of cinchonine and cinchonidine, *J. Photochem. Photobiol. A: Chem.*, 1993, **75**, 137-141.

3 W. Qin, A. Vozza and A. M. Brouwer, Photophysical properties of cinchona organocatalysts in organic solvents, *J. Phys. Chem. C*, 2009, **113**, 11790-11795.

4 T. Kumpulainen and A. M. Brouwer, Excited-state proton transfer and ion pair formation in a Cinchona organocatalyst, *Phys. Chem. Chem. Phys.*, 2012, **14**, 13019-13026.

5 D. V. O'Connor, S. R. Meech and D. Phillips, Complex fluorescence decay of quinine bisulphate in aqueous sulphuric acid solution, *Chem. Phys. Lett.*, 1982, **88**, 22-26.

6 N. P. Illsley and A. S. Verkman, Membrane chloride transport measured using a chloride-sensitive fluorescent probe, *Biochemistry*, 1987, **26**, 1215-1219.

7 R. D. Schwartz and X. Yu, Optical imaging of intracellular chloride in living brain slices, *J. Neurosci. Methods*, 1995, **62**, 185-192.

8 J. R. Inglefield and R. D. Schwartz-Bloom, Fluorescence imaging of changes in intracellular chloride in living brain slices, *Methods Companion Methods Enzymol.*, 1999, **18**, 197-203.

9 B. Hennig, G. Schultheiss, K. Kunzelmann and M. Diener, Ca2+-induced Cl- efflux at rat distal colonic epithelium, *J. Membr. Biol.*, 2008, **221**, 61-72.

10 V. Amendola, L. Fabbrizzi and E. Monzani, A concave fluorescent sensor for anions based on 6-methoxy-1-methylquinolinium, *Chem. Eur. J.*, 2004, **10**, 76-82.

11 L. Baù, F. Selvestrel, M. Arduini, I. Zamparo, C. Lodovichi and F. Mancin, A cell-penetrating ratiometric nanoprobe for intracellular chloride, *Org. Lett.*, 2012, **14**, 2984-2987.

12 S. Jayaraman and A. S. Verkman, Quenching mechanism of quinolinium-type chloride-sensitive fluorescent indicators, *Biophys. Chem.*, 2000, **85**, 49-57.

13 M. S. Mehata and H. B. Tripathi, Fluorescence quenching of 6-methoxyquinoline: an indicator for sensing chloride ion in aqueous media, *J. Luminesc.*, 2002, **99**, 47-52.

14 R. Krapf, N. P. Illsley, H. C. Tseng and A. S. Verkman, Structure-activity relationships of chloride-sensitive fluorescent indicators for biological application, *Anal. Biochem.*, 1988, **169**, 142-150.

15 J. Biwersi and A. S. Verkman, Cell-permeable fluorescent indicator for cytosolic chloride, *Biochemistry*, 1991, **30**, 7879-7883.

16 D. H. Macartney, Encapsulation of drug molecules by cucurbiturils: Effects on their chemical properties in aqueous solution, *Isr. J. Chem.*, 2011, **51**, 600-615.

17 K. M. Park, K. Suh, H. Jung, D. W. Lee, Y. Ahn, J. Kim, K. Baek and K. Kim, Cucurbituril-based nanoparticles: a new efficient vehicle for targeted intracellular delivery of hydrophobic drugs, *Chem. Commun.*, 2009, 71-73.

18 V. D. Uzunova, C. Cullinane, K. Brix, W. M. Nau and A. I. Day, Toxicity of cucurbit[7]uril and cucurbit[8]uril: an exploratory in vitro and in vivo study, *Org. Biomol. Chem.*, 2010, **8**, 2037-2042.

19 G. Hettiarachchi, D. Nguyen, J. Wu, D. Lucas, D. Ma, L. Isaacs and V. Briken, Toxicology and drug delivery by cucurbit[n]uril type molecular containers, *Plos One*, 2010, **5**, e10514.

20 P. Montes-Navajas, M. Gonzalez-Bejar, J. C. Scaiano and H. Garcia, Cucurbituril complexes cross the cell membrane, *Photochem. Photobiol. Sci.*, 2009, **8**, 1743-1747.

21 R. N. Dsouza, U. Pischel and W. M. Nau, Fluorescent dyes and their supramolecular host/guest complexes with macrocycles in aqueous solution, *Chem. Rev.*, 2011, **111**, 7941-7980.

22 C. D. Geddes, K. Apperson and D. J. S. Birch, New fluorescent quinolinium dyes — applications in nanometre particle sizing, *Dyes Pigments*, 2000, **44**, 69-74.

23 A. Day, A. P. Arnold, R. J. Blanch and B. Snushall, Controlling factors in the synthesis of cucurbituril and its homologues, *J. Org. Chem.*, 2001, **66**, 8094-8100.

24 W. H. Melhuish, Quantum efficiencies of fluorescence of organic substances: Effect of solvent and concentration of the fluorescent solute, *J. Phys. Chem.*, 1961, **65**, 229-235.

25 M. Megyesi and L. Biczók, Considerable change of fluorescence properties upon multiple binding of coralyne to 4-sulfonatocalixarenes, *J. Phys. Chem. B*, 2010, **114**, 2814-2819.

26 V. Wintgens, L. Biczók and Z. Miskolczy, Thermodynamics of inclusion complex formation between 1-alkyl-3-methylimidazolium ionic liquids and cucurbit[7]uril, *Supramol. Chem.*, 2010, **22**, 612-618.

27 R. F. Chen, Some characteristics of the fluorescence of quinine, *Anal. Biochem.*, 1967, **19**, 374-387.

28 S. Joshi, Y. T. Varma and D. D. Pant, Steady state and time-resolved fluorescence spectroscopy of quinine sulfate dication in ionic and neutral micelles: Effect of

micellar charge on photophysics, *Colloids Surfaces A: Physicochem. Eng. Aspects*, 2013, **425**, 59-67.

29 A. N. Fletcher, Fluorescence emission band shift with wavelength of excitation, *J. Phys. Chem.*, 1968, **72**, 2742-2749.

30 I. Balomenou and G. Pistolis, Experimental evidence for a highly reversible excited state equilibrium between s-cis and s-trans rotational isomers of 2-methoxynaphthalene in solution, *J. Am. Chem. Soc.*, 2007, **129**, 13247-13253.

31 M. Albrecht, C. Bohne, A. Granzhan, H. Ihmels, T. C. S. Pace, A. Schnurpfeil, M. Waidelich and C. Yihwa, Dual fluorescence of 2-methoxyanthracene derivatives, *J. Phys. Chem. A*, 2007, **111**, 1036-1044.

32 S. R. Salman, Carbon-13 chemical shift and the conformation of substituted naphthalenes, *Spectrochimica Acta Part A: Molecular Spectroscopy*, 1984, **40**, 229-232.

33 A. S. R. Koti, M. M. G. Krishna and N. Periasamy, Time-resolved area-normalized emission spectroscopy (TRANES): A novel method for confirming emission from two excited states, *J. Phys. Chem. A*, 2001, **105**, 1767-1771.

34 D. Pant, H. B. Tripathi and D. D. Pant, Photophysics of protonated 6-methoxyquinoline: steady state and time-dependent fluorescence, *J. Photochem. Photobiol. A: Chem.*, 1990, **54**, 239-249.

35 D. Pant, H. B. Tripathi and D. D. Pant, Photophysics of quinidine dication in relation to quinine dication and 6-methoxyquinoline monocation, *J. Luminesc.*, 1991, **50**, 249-257.

36 D. Pant, H. B. Tripathi and D. D. Pant, Excited state solvation dynamics of 6-methoxyquinoline, *J. Photochem. Photobiol. A: Chem.*, 1991, **56**, 207-217.

37 D. Pant, U. C. Tripathi, G. C. Joshi, H. B. Tripathi and D. D. Pant, Photophysics of doubly-charged quinine: Steady state and time-dependent fluorescence, *J. Photochem. Photobiol. A: Chem.*, 1990, **51**, 313-325.

38 B. Valeur, *Molecular Fluorescence, Principles and Applications*, Wiley-VCH, Weinheim, 2002.

39 C. Marquez and W. M. Nau, Polarizabilities inside molecular containers, *Angew. Chem. Int. Ed.*, 2001, **40**, 4387-4390.

40 I. Loeff, J. Rabani, A. Treinin and H. Linschitz, Charge transfer and reactivity of nπ* and ππ* organic triplets, including anthraquinonesulfonates, in interactions with inorganic anions: a comparative study based on classical Marcus theory, *J. Am. Chem. Soc.*, 1993, **115**, 8933-8942.

41 D. Rehm and A. Weller, Kinetics of fluorescence quenching by electron and H-atom transfer, *Isr. J. Chem.*, 1970, **8**, 259-271.

42 R. G. Bates and J. B. Macaskill, Standard potential of the silver-silver chloride electrode, *Pure Appl. Chem.*, 1978, **50**, 1701-1706.

43 V. Avila, C. M. Previtali and C. A. Chesta, Free energy dependence of the diffusion-limited quenching rate constants in photoinduced electron transfer processes, *Photochem. Photobiol. Sci.*, 2008, **7**, 104-108.

44 C. Marquez, F. Huang and W. M. Nau, Cucurbiturils: Molecular nanocapsules for time-resolved fluorescence-based assays, *IEEE Trans. Nanobiosci.*, 2004, **3**, 39-45.

45 Z. Miskolczy and L. Biczók, Inclusion complex formation of ionic liquids with 4-sulfonatocalixarenes studied by competitive binding of berberine alkaloid fluorescent probe, *Chem. Phys. Lett.*, 2009, **477**, 80-84.

46 C. Márquez, R. R. Hudgins and W. M. Nau, Mechanism of host−guest complexation by cucurbituril, *J. Am. Chem. Soc.*, 2004, **126**, 5806-5816.

47 W. Ong and A. E. Kaifer, Salt effects on the apparent stability of the cucurbit[7]uril−methyl viologen inclusion complex, *J. Org. Chem.*, 2004, **69**, 1383-1385.

48 M. Megyesi, L. Biczók and I. Jablonkai, Highly sensitive fluorescence response to inclusion complex formation of berberine alkaloid with cucurbit[7]uril, *J. Phys. Chem. C*, 2008, **112**, 3410-3416.

49 T. Wiseman, S. Williston, J. F. Brandts and L.-N. Lin, Rapid measurement of binding constants and heats of binding using a new titration calorimeter, *Anal. Biochem.*, 1989, **179**, 131-137.

50 W. B. Turnbull and A. H. Daranas, On the value of c: Can low affinity systems be studied by isothermal titration calorimetry?, *J. Am. Chem. Soc.*, 2003, **125**, 14859-14866.

51 B. W. Sigurskjold, Exact analysis of competition ligand binding by displacement isothermal titration calorimetry, *Anal. Biochem.*, 2000, **277**, 260-266.

52 Z. Miskolczy, L. Biczók, M. Megyesi and I. Jablonkai, Inclusion complex formation of ionic liquids and other cationic organic compounds with cucurbit[7]uril studied by 4',6-diamidino-2-phenylindole fluorescent probe, *J. Phys. Chem. B*, 2009, **113**, 1645-1651.

53 F. Biedermann, V. D. Uzunova, O. A. Scherman, W. M. Nau and A. De Simone, Release of high-energy water as an essential driving force for the high-affinity binding of cucurbit[n]urils, *J. Am. Chem. Soc.*, 2012, **134**, 15318-15323.

54 J. W. Lee, S. Samal, N. Selvapalam, H. J. Kim and K. Kim, Cucurbituril homologues and derivatives: New opportunities in supramolecular chemistry, *Acc. Chem. Res.*, 2003, **36**, 621-630.

55 J. J. Delpuech, in *Dynamics of solutions and fluid mixtures by NMR*, ed. J. J. Delpuech, Wiley, New York, 1995, pp. 73-172.---

56 J. S. Yu, F. G. Wu, L. F. Tao, J. J. Luo and Z. W. Yu, Mechanism of the fast exchange between bound and free guests in cucurbit[7]uril-guest systems, *Phys. Chem. Chem. Phys.*, 2011, **13**, 3638-3641.

57 S. L. Murov, I. Carmichael and G. L. Hug, eds., *Handbook of photochemistry*, Marcel Dekker, New York, 1993.

58 J. van Stam, S. De Feyter, F. C. De Schryver and C. H. Evans, 2-Naphthol complexation by β-cyclodextrin: Influence of added short linear alcohols, *J. Phys. Chem.*, 1996, **100**, 19959-19966.

59 M. Christoff, L. T. Okano and C. Bohne, Dynamics of complexation of flavone and chromone to β-cyclodextrin, *J. Photochem. Photobiol. A: Chem.*, 2000, **134**, 169-176.

60 H. Tang, D. Fuentealba, Y. H. Ko, N. Selvapalam, K. Kim and C. Bohne, Guest binding dynamics with cucurbit[7]uril in the presence of cations, *J. Am. Chem. Soc.*, 2011, **133**, 20623-20633.

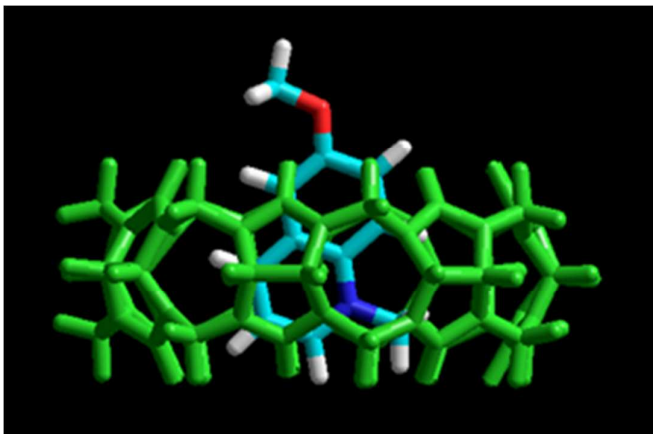

Graphical abstact

The inclusion of 6-methoxy-1-methylquinolinium in cucurbit[7]uril decelerates electron transfer but does not affect torsional isomerization.

SUPPORTING INFORMATION

Effect of torsional isomerization and inclusion complex formation with cucurbit[7]uril on the fluorescence of 6-methoxy-1-methylquinolinium

Zsombor Miskolczy[a], József G. Harangozó[a], László Biczók[a*], Véronique Wintgens[b], Cédric Lorthioir[b], Catherine Amiel[b]

[a]*Institute of Molecular Pharmacology, Research Centre for Natural Sciences, Hungarian Academy of Sciences, P.O. Box 17, 1525 Budapest, Hungary*

[b]*Systèmes Polymères Complexes, ICMPE, 2 rue Henri Dunant, 94320 Thiais, France*

Figure S1. Absorption (A) and fluorescence spectrum (B) of C_1MQ in water (blue line) and quinine sulfate in 0.5 M H_2SO_4 aqueous solution (red line). Excitation at 350 nm.

Figure S2. Time-resolved area-normalized emission spectrum (TRANES) and excitation spectrum of *cis*- and *trans*-C_1MQ in water.

Figure S3. Time-resolved area-normalized emission spectrum (TRANES) of 0.043 mM C_1MQ and 0.316 mM CB7 in aqueous solution at 0 (red), 50 (black) and 100 ns (blue) after excitation at 370 nm.

Figure S4. 400 MHz ^{1}H COSY spectrum of C_1MQ in DMSO at 298 K.

Figure S5. 400 MHz ^{1}H NOESY spectrum of C_1MQ in DMSO at 298 K. The mixing time value was set to 800 ms.

* Corresponding author. Phone: +36-1438-1103; Fax: +36-1438-1143; E-mail: biczok.laszlo@ttk.mta.hu

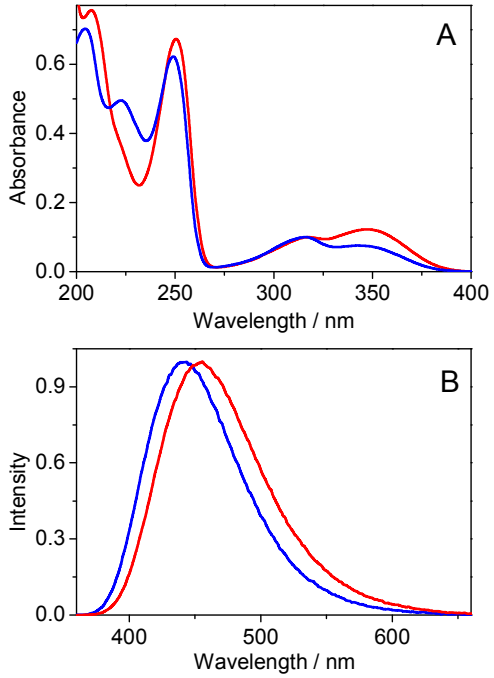

Figure S1. Absorption (A) and fluorescence spectrum (B) of C_1MQ in water (blue line) and quinine sulfate in 0.5 M H_2SO_4 aqueous solution (red line). Excitation at 350 nm.

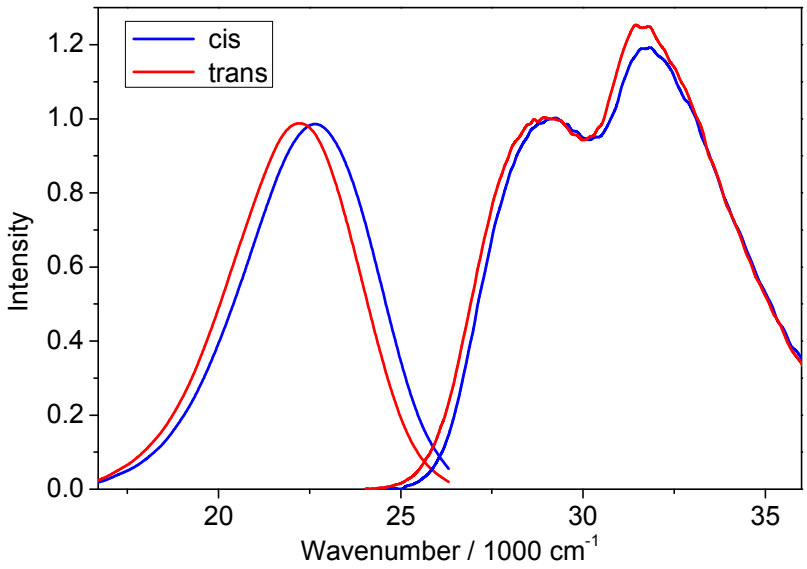

Figure S2. Time-resolved area-normalized emission spectrum (TRANES) and excitation spectrum of *cis*- and *trans*-C_1MQ in water.

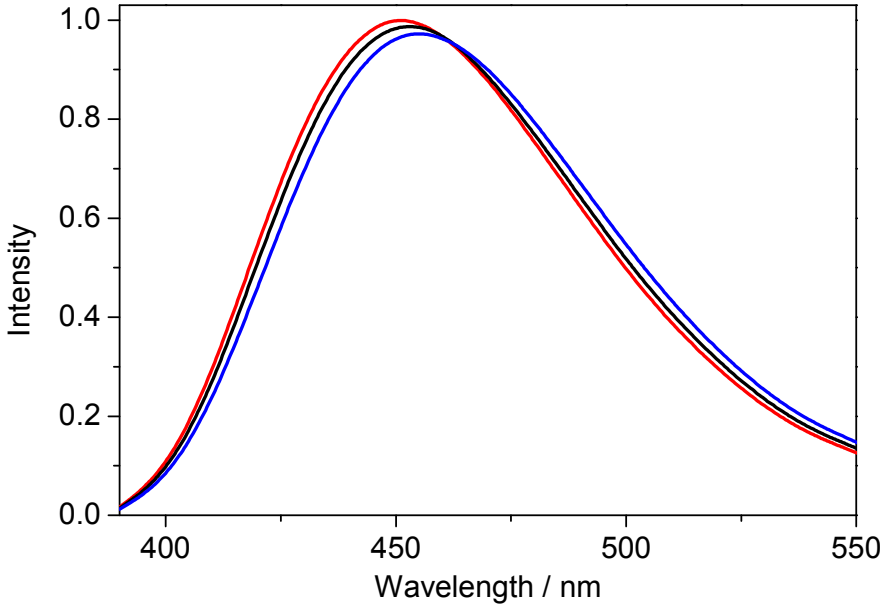

Figure S3. Time-resolved area-normalized emission spectrum (TRANES) of 0.043 mM C_1MQ and 0.316 mM CB7 in aqueous solution at 0 (red), 50 (black) and 100 ns (blue) after excitation at 370 nm.

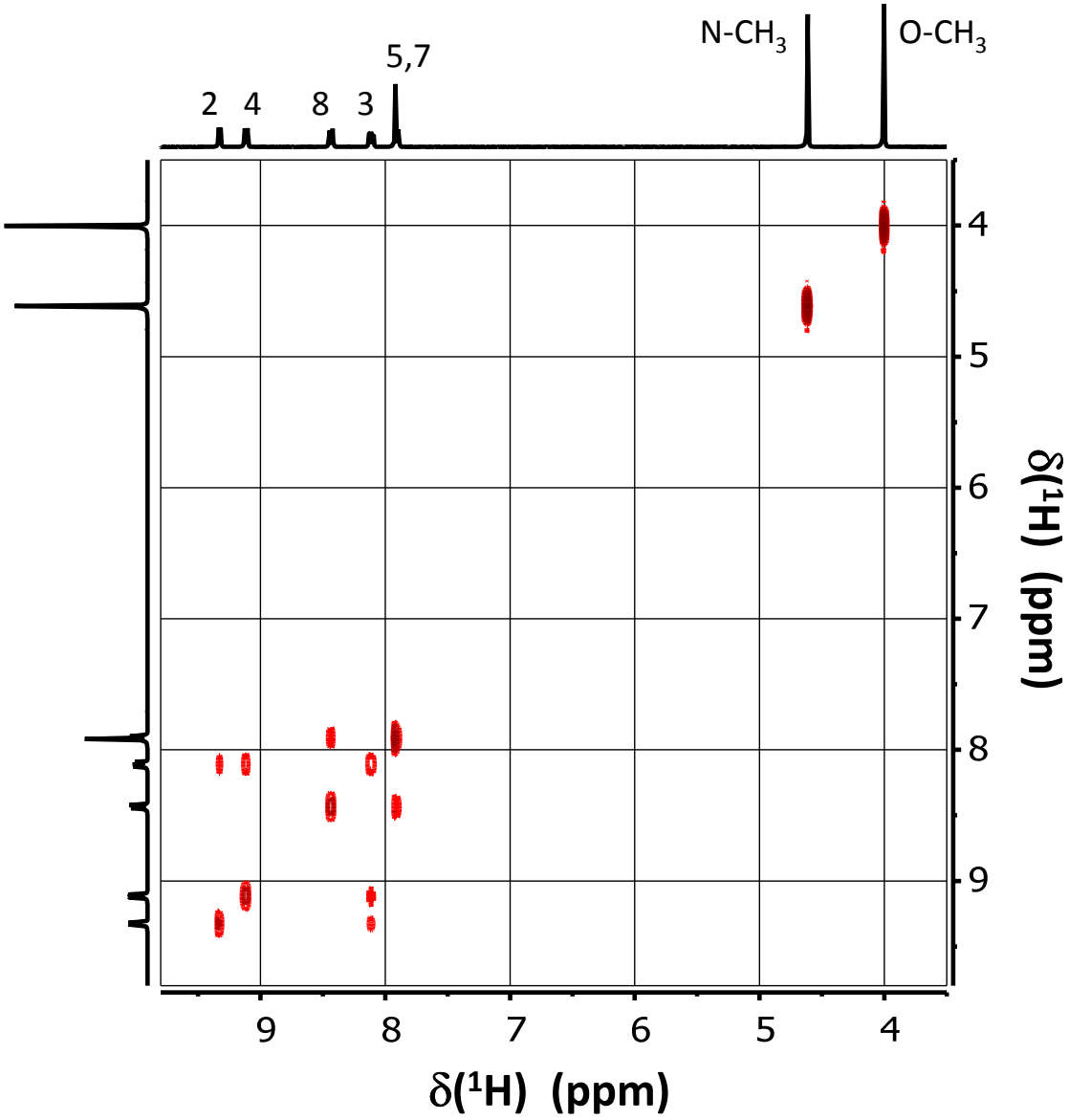

Figure S4. 400 MHz ^{1}H COSY spectrum of C_1MQ in DMSO at 298 K.

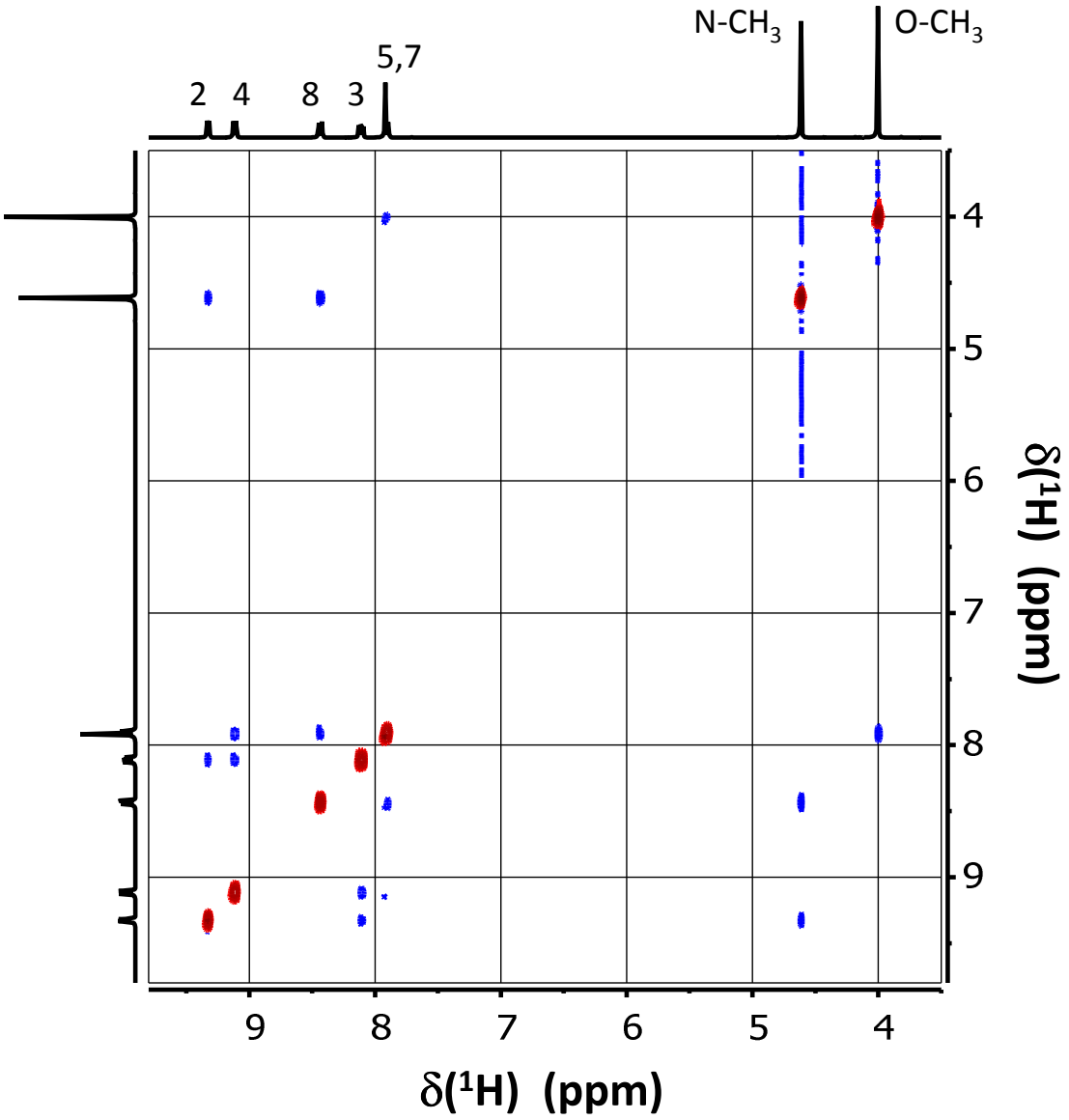

Figure S5. 400 MHz ^{1}H NOESY spectrum of C_1MQ in DMSO at 298 K. The mixing time value was set to 800 ms.